EBioMedicine 20 (2017) 39–49

Contents lists available at ScienceDirect

EBioMedicine

journal homepage: www.ebiomedicine.com

Research Paper

A Specific Mutational Signature Associated with DNA 8-Oxoguanine Persistence in MUTYH-defective Colorectal Cancer

Alessandra Viel [a,1], Alessandro Bruselles [b,1], Ettore Meccia [c,1], Mara Fornasarig [d], Michele Quaia [a], Vincenzo Canzonieri [e], Eleonora Policicchio [f], Emanuele Damiano Urso [g], Marco Agostini [g,h], Maurizio Genuardi [i,j], Emanuela Lucci-Cordisco [i], Tiziana Venesio [k], Aline Martayan [l], Maria Grazia Diodoro [l], Lupe Sanchez-Mete [l], Vittoria Stigliano [l], Filomena Mazzei [c], Francesca Grasso [c], Alessandro Giuliani [c], Marta Baiocchi [b], Roberta Maestro [a], Giuseppe Giannini [m], Marco Tartaglia [f,2], Ludmil B. Alexandrov [n,o,p], Margherita Bignami [c,2,*]

[a] Functional Onco-Genomics and Genetics, CRO Aviano National Cancer Institute, Aviano, Italy
[b] Department of Haematology, Oncology and Molecular Medicine, Istituto Superiore di Sanità, Rome, Italy
[c] Department of Environment and Primary Prevention, Istituto Superiore di Sanità, Rome, Italy
[d] Unit of Gastroenterology, CRO Aviano National Cancer Institute, Aviano, Italy
[e] Unit of Pathology, CRO Aviano National Cancer Institute, Aviano, Italy
[f] Genetics and Rare Diseases Research Division, Ospedale Pediatrico Bambino Gesù, Rome, Italy
[g] First Surgical Clinic, Department of Surgical, Oncological and Gastroenterological Sciences, University of Padua, Padua, Italy
[h] Nano Insperid Biomedicine Lab, Istituto di Ricerca Pediatrica (IRP) Padua, Italy
[i] Institute of Genomic Medicine, Catholic University, Rome, Italy
[j] Fondazione Policlinico Universitario "A. Gemelli, Rome, Italy
[k] Unit of Pathology, Candiolo Cancer Institute-FPO, IRCCS, Candiolo, Turin, Italy
[l] Division of Gastroenterology and Digestive Endoscopy, Regina Elena National Cancer Institute, Rome, Italy
[m] Department of Molecular Medicine, University La Sapienza, Rome, Italy
[n] Theoretical Biology and Biophysics, Los Alamos National Laboratory, Los Alamos, NM, USA
[o] Center for Nonlinear Studies, Los Alamos National Laboratory, Los Alamos, NM, USA
[p] University of New Mexico Comprehensive Cancer Center, Albuquerque, NM 87102, USA

ARTICLE INFO

Article history:
Received 17 February 2017
Received in revised form 7 April 2017
Accepted 11 April 2017
Available online 13 April 2017

Keywords:
MUTYH-associated polyposis
Colorectal cancer
8-Oxoguanine
Base excision repair
Exome sequencing
Mutational signature

ABSTRACT

8-Oxoguanine, a common mutagenic DNA lesion, generates G:C>T:A transversions via mispairing with adenine during DNA replication. When operating normally, the MUTYH DNA glycosylase prevents 8-oxoguanine-related mutagenesis by excising the incorporated adenine. Biallelic *MUTYH* mutations impair this enzymatic function and are associated with colorectal cancer (CRC) in MUTYH-Associated Polyposis (MAP) syndrome. Here, we perform whole-exome sequencing that reveals a modest mutator phenotype in MAP CRCs compared to sporadic CRC stem cell lines or bulk tumours. The excess G:C>T:A transversion mutations in MAP CRCs exhibits a novel mutational signature, termed Signature 36, with a strong sequence dependence. The MUTYH mutational signature reflecting persistent 8-oxoG:A mismatches occurs frequently in the *APC*, *KRAS*, *PIK3CA*, *FAT4*, *TP53*, *FAT1*, *AMER1*, *KDM6A*, *SMAD4* and *SMAD2* genes that are associated with CRC. The occurrence of Signature 36 in other types of human cancer indicates that DNA 8-oxoguanine-related mutations might contribute to the development of cancer in other organs.

1. Introduction

DNA repair provides a major protection against cancer, and germline DNA repair defects in inherited syndromes confer a significant cancer predisposition. DNA replication errors are a major source of mutations, and early-onset colorectal and other cancers are associated with germline mutations in DNA mismatch repair (MMR) genes (Lynch et al., 2015) or in the proofreading exonuclease domains of DNA

* Corresponding author.
E-mail address: margherita.bignami@gmail.com (M. Bignami).
[1] These authors equally contributed to this work.
[2] These authors jointly supervised this work.

http://dx.doi.org/10.1016/j.ebiom.2017.04.022

polymerases POLE and POLD1 (Palles et al., 2013). In a distinct mutational mechanism, endogenously or exogenously generated reactive oxygen species (ROS) induce pre-mutagenic DNA lesions. Most ROS-induced base damage is repaired by base excision repair (BER) initiated by DNA glycosylases. 8-Oxoguanine (8-oxoG), one of the most common oxidative DNA lesions can mispair with adenine during DNA replication to generate G:C>T:A transversion mutations. 8-oxoG-induced mutagenesis is prevented by the cooperative action of the DNA glycosylases encoded by the *OGG1* and *MUTYH* genes. OGG1 removes 8-oxoG from 8-oxoG:C pairs and MUTYH scans the newly-synthesized daughter strand to locate and remove incorporated adenine mispaired with 8-oxoG (Mazzei et al., 2013; Markkanen et al., 2013; Tsuzuki et al., 2007). A hydrolase encoded by the *MTH1* gene provides a third level of protection against oxidative mutagenesis by degrading 8-oxodGTP to prevent the incorporation of 8-oxodGMP into DNA (Mo et al., 1992). Inactivation of any of these genes increases steady-state DNA 8-oxoG levels and confers a mutator phenotype (Klungland et al., 1999; Tsuzuki et al., 2001; Hirano et al., 2003).

To date, no human disease has been associated with defective OGG1 or MTH1 activities. In contrast, germline biallelic *MUTYH* mutations underlie *MUTYH*-associated polyposis (MAP), a recessively heritable colorectal polyposis with a predisposition to colorectal cancer (CRC) (Al-Tassan et al., 2002; Sieber et al., 2003). CRCs in MAP patients bear distinctive somatic G:C>T:A transversions in the *APC* gene (Al-Tassan et al., 2002; Sieber et al., 2003; Jones et al., 2002). The relationship between defective repair of oxidized DNA and CRC susceptibility was strengthened by the recent report that germline mutations in *NTHL1*, encoding a DNA glycosylase involved in the BER of oxidized pyrimidines are associated with a polyposis clinically similar to MAP (Weren et al., 2015). Thus, two repair pathways counteract CRC susceptibility by acting at replication to process mismatches containing oxidized DNA bases.

Mutational signatures in cancer genomes provide indications of the mechanisms underlying neoplastic transformation (Alexandrov, 2015; Alexandrov et al., 2013a,b, 2015; Helleday et al., 2014). Thus, CRC from MAP patients offer the unique opportunity to identify a mutational fingerprint of persistent 8-oxoG:A mismatches. Here, we report that whole-exome DNA sequencing identifies a distinct mutational signature of G:C>T:A transversions in MAP CRC. The mutational signature is reflected in the specific pattern of oncogenes/tumour suppressors involved in colorectal carcinogenesis and associated with inactive MUTYH. Our findings also indicate the possible involvement of DNA oxidation-related mutations in other types of human cancer as the *MUTYH* mutational fingerprint is present in cancers of other organs.

2. Material and Methods

2.1. Subjects and Tissue Samples

All subjects included in this study gave informed consent for gene testing and related research (Table S1). The local scientific IRB approved the collection and usage of tumour samples for this research (CRO Aviano IRB-03-2016). Blood, normal intestinal mucosa, adenomas and CRCs were retrospectively obtained from MAP patients with confirmed constitutional biallelic mutations in the *MUTYH* gene. CRCs were collected at surgery, while adenomas and normal mucosa were harvested at colectomy or endoscopic polypectomy. In all cases histopathological evaluation was performed by a pathologist.

DNA from frozen tissues was extracted using the Qiagen DNeasy Tissue kit (Qiagen, Hilden, Germany) with a protocol including RNase treatment. FFPE tissues were deparaffinized by two washes in Noxyl (15 min at 56 °C) and DNA was then obtained using the FFPE Qiagen Tissue kit (Qiagen). DNA quality and concentrations were assessed using Nanodrop spectrophotometer (ThermoFischer Scientific, MA, USA) and Qubit Fluorometer (Invitrogen, CA, USA).

2.2. Whole Exome Sequencing, Data Analysis and Validation

Whole Exome Sequencing was performed by the Beijing Genomics Institute (BGI, Hong Kong). Target enrichment was performed using in-solution technology (NimbleGen SeqCap EZ Library v.3.0, Roche) and the resulting target libraries were sequenced by Illumina sequencing technology (HiSeq2000) (Illumina, San Diego, CA, USA). Raw image files were processed by Illumina base calling software (CASAVA 1.7) using default parameters. Paired-end reads were aligned to the human genome (UCSC GRCh37/hg19) with the Burrows-Wheeler aligner (BWA v. 0.7.10). Presumed PCR duplicates were removed using Picard's MarkDuplicates. The Genome Analysis Toolkit (GATK 3.2) was used for realignment of sequences encompassing indels and for base quality recalibration. Somatic single-nucleotide variants were detected using muTect software v.1.1.6, and small indels were identified through a comparison between indels called in individual CRCs and their matched non-tumoural samples by means of the GATK Haplotype Caller algorithm, applying the following quality filters: quality score > 100 and quality-by-depth score > 1.5; indels below these thresholds or resulting from four or more reads having ambiguous mapping (this number being >10% of all aligned reads) were discarded. The resulting SNVs and small indels were annotated by SnpEff v3.6 and dbNSFP2.8 in terms of functional impact of variants (missense or nonsense, coding or non-coding, location with respect to exon-intron junction, depth, reference/variant reads ratio, dbSNP ID, amino acid change and position, cancer association data and structural/functional impact). Variant validation and genotyping were performed by Sanger sequencing. Amplicons were directly sequenced using the ABI BigDye Terminator Sequencing kit (Applied Biosystems, Foster City, CA, USA) and an automated capillary sequencer (ABI 3500, Applied Biosystems). Sequence electropherograms were analyzed using Sequencing Analysis Software v.5.4 (Applied Biosystems).

2.3. Microsatellite Instability Analysis

Five mononucleotide and two pentanucleotide markers were co-amplified using the MSI analysis system (Promega Madison, WI, USA) according to the manufacturer's protocol. The fluorescent-labeled PCR products obtained from constitutional DNA and tumour DNA were separated by capillary electrophoresis using an AB3130 xl sequencer and evaluated with the GeneMapper software (Applied Biosystems/Life technologies). The 5 quasi-monomorphic mononucleotide markers included in the kit have high sensitivity and specificity in detecting alterations in tumour samples with mismatch repair defects. Criteria for definition of MSS and MSI are according to the Bethesda guidelines (Umar et al., 2004).

2.4. Mutational Signature Analysis

Prior to performing mutational signatures analysis, the mutational catalogues of all examined samples were generated. These catalogues include the six types of substitutions (C>A, C>G, C>T, T>A, T>C, T>G; mutations are referred to by the pyrimidine of the mutated Watson–Crick base pair) as well as the base immediately 5′ and the base immediately 3′ of each somatic mutation. The immediate 5′ and 3′ sequence context for each somatic mutation was extracted using the ENSEMBL Core APIs for human genome build GRCh37.

Mutational signatures analysis was performed based on somatic substitutions and their immediate sequence context. Briefly, mutational signatures were deciphered for all cancer types together using our previously developed computational MATLAB framework (Alexandrov et al., 2013a).

The computational framework for deciphering mutational signatures is freely available and it can be downloaded from: http://www.mathworks.com/matlabcentral/fileexchange/38724. The algorithm deciphers the minimal set of mutational signatures that optimally explains

the proportion of each mutation type found in each catalogue and then estimates the contribution of each signature to each mutational catalogue. Overall, we identified multiple distinct mutational signatures, most of which were previously reported by others or us (Alexandrov et al., 2013a,b; Schulze et al., 2015). The names of mutational signatures used in this manuscript are consistent with the ones on the COSMIC website, http://cancer.sanger.ac.uk/cosmic/signatures.

2.5. Target Re-sequencing

A TruSeq Custom Amplicon (TSCA) workflow was applied for interrogating targeted regions of interest in a series of MAP tumours. The custom panel included all exons and ±10 padding intronic regions of the following target genes: *AMER1*, *APC*, *FAT1*, *FAT4*, *KDM6A*, *KRAS*, *PIK3CA*, *SMAD2*, *SMAD4*, *TP53*. A project of 632 amplicons having a median size of 175 bp was constructed and optimized using Design Studio tool (Illumina). These amplicons covered a cumulative target of 60,174 bp and, according to the design, there were only 13 gaps, with a predicted 97% in silico-coverage of the region of interest. Double stranded DNA (250 ng) from frozen tissues and DNA from FFPE tissues (250–500 ng) were used for library preparation according to the TSCA protocol (Illumina). After normalization, three pooled quantified libraries were sequenced on the MiSeq platform (Illumina) using the 2 × 175 configuration and run on a MiSeq Reagent kit V3 sequencing flow cell with 175-cycle paired-end run plus two eight-cycle index reads. Data were automatically aligned using the MiSeq Reporter and visualized using Illumina Amplicon Viewer (Illumina) and Integrative Genomics Viewer 2.3 (Broad Institute, Boston, U.S.A.). The vcf files were imported into Illumina VariantStudio v2.2 software and analyzed with the default setting. SNV and in/del variants were annotated using different filtering options. Briefly, a) variant call quality was based on the selection of the "PASS" filter; b) to narrow results to the somatic events, annotation of the vast majority of constitutional variants was avoided by filtering only variants with global Minor Allele Frequency < 1 and discarding variants recurrent in more tumour tissues of the same individual; c) frequency of the alternative allele was set at a threshold of 5%; d) the "consequence" option was used to filter data by variants that alter the coding potential of the transcript, i.e. frameshift, stop gained, initiator codon, inframe insertion or deletion, splice and missense with deleterious (SIFT) or damaging (Polyphen) prediction; synonymous, intronic, 5′- and 3′- UTR and missense variants with tolerated (SIFT) and benign (Polyphen) prediction were filtered out, unless they were reported in the Catalogue of somatic mutations in cancer (Cosmic) database (http://cancer.sanger.ac.uk/cosmic).

2.6. MUTYH Glycosylase Assays

Two DNA duplexes, each containing a single 8-oxodG:A mismatch with different flanking sequences, were used as substrates for adenine DNA glycosylase assays. HPLC-purified 30-mer oligonucleotides (5′-CTT GCC TAC GCC ACA AGC TCC AAC TAC CAC and 5′-CTT GCC TAC GCC AAC AGC TCC AAC TAC CAC), 3′-end labeled with 6-carboxyfluorescein (6-FAM) were annealed to the complementary strands containing a single 8-oxodG (at 16 nt and 17 nt from their 5'end.) All oligonucleotides were from Thermo Fisher Scientific (Thermo Fisher Scientific GmbH, Ulm, Germany). To obtain human purified MUTYH, *Escherichia coli* strain BL21 CodonPlus (DE3) RIPL (Stratagene, La Jolla, CA, USA) competent cells were transformed with a pMAL-c4E vector containing the *MUTYH*-cDNA. Bacteria were grown at 37 °C in Luria Broth medium with 5 g/l of glucose until OD 600 nm = 0.6 and then induced with 0.4 mM isopropyl-β-D-thiogalactopyranoside (IPTG) for 3 h at 25 °C. Cells were harvested and resuspended in phosphate-buffered saline (PBS) (1/40th of culture volume). In all, 5 mM dithiothreitol (DTT), 1 mg/ml of lysozyme and protease inhibitors (Roche) were added to the cell suspension and incubated for 30 min on ice. Lysates were cleared by centrifugation and the supernatant loaded on an amylose column (New England BioLabs Inc., Ipswich, MA). The maltose binding protein (MBP)-MUTYH fusion protein was eluted in 10 mM Tris–HCl, pH 7.5, 10 mM maltose buffer. Protein containing fractions were analyzed by sodium dodecyl sulphate–polyacrylamide gel electrophoresis (SDS–PAGE) and stained with Comassie blue dye. Protein recovery was evaluated by gel analysis by ImageJ software, available free online at the NIH website (http://rsb.info.nih.gov/). MUTYH active fraction was evaluated as described before (Turco et al., 2013). In single-turnover conditions ([MUTYH]»[DNA]), DNA substrate (10 nM) was reacted with an active protein (20 nM). Aliquots were withdrawn at different times, ranging from 30s to 10 min, and reaction was stopped by addition of NaOH (80 mM) and heating at 90 °C for 4 min. Reaction products were separated by denaturing PAGE. Gel images were acquired by Typhoon 9600 scanner (GE Healthcare, Uppsala, Sweden) and analysis performed by *Image J* and *Kaleidagraph* software (Synergy software).

2.7. Statistical Analysis

The mutation profiles were analyzed by means of principal Component Analysis of the matrix having as statistical units the different types of mutations and as variables the samples.

3. Results

3.1. Determination of Somatic Mutation Frequencies by Exome Sequencing in MAP CRC

Whole-exome DNA sequencing was performed on seven matched CRC/normal mucosa pairs from six unrelated MAP patients. These individuals harbour either the p.Gly396Asp and p.Tyr179Cys variants that are common among Caucasians or the p.Arg245His, p.Gly264Trpfs*7 and p.Glu480del that occur relatively frequently in Italian MAP patients (Aretz et al., 2014). A summary of the constitutional *MUTYH* genotypes, clinical phenotypes and pathology reports is listed in Table S1. The age of cancer diagnosis in these MAP patients is quite ample with a range of 27–73 years, in accordance with a recent Italian survey (Ricci et al., 2017). All these variants compromise MUTYH activity and are associated with increased steady-state levels of DNA 8-oxoG in lymphoblastoid cell lines (Molatore et al., 2010; D'Agostino et al., 2010; Ruggieri et al., 2013; Grasso et al., 2014).

The number of somatic non-synonymous single nucleotide variants (SNVs) and small insertions/deletions (indels) was similar among MAP CRCs, with a median value of 340 mutations per sample (range: 247–423). The mutational landscape of MAP tumours was compared to a set of 23 well-characterized colorectal cancer stem cell lines (CSCs) previously shown to faithfully reproduce the genomic complexity of CRC (De Angelis et al., 2016). As expected, the number of mutations in these CSCs was dependent on MMR status, with median values of 210 and 2215 mutations/exome in MMR-proficient (MSS) and MMR–deficient (MSI) CSCs, respectively. These values correspond to 3.5 ± 0.3 and 34.6 ± 6.9 mutations per Mb for MSS and MSI CSCs, respectively (Fig. 1A and B) and are in good agreement with those reported by The Cancer Genome Atlas Network (2012). MAP tumours contained 5.3 ± 0.38 mutations per Mb, an increase of 1.5-fold over the frequency in MMR-proficient CSCs (Fig. 1A). Approximate values for mutation rates were derived by dividing the number of somatic mutations per tumour by the age of the patient at diagnosis (Tomasetti et al., 2015). Median ages of cancer diagnosis were 47 in MAP patients and 73 years for CSCs (range: 27–73 and 47–88 years, respectively). The mutation rate in MAP CRCs (6.8 ± 0.6) was 2-fold higher than that in MSS CSCs (3.3 ± 0.3) (p-value = 2.4×10^{-5}; Fig. 1C). In contrast MSI CSCs were characterized by an extreme value of 31.7 ± 6 with an almost 10-fold increase over MSS CSCs (data not shown).

The higher frequency of mutations in MAP tumours was driven predominantly by an increase in SNVs and the number of indels was relatively low compared to either MSS or MSI CSCs (Fig. 1D). MSI is

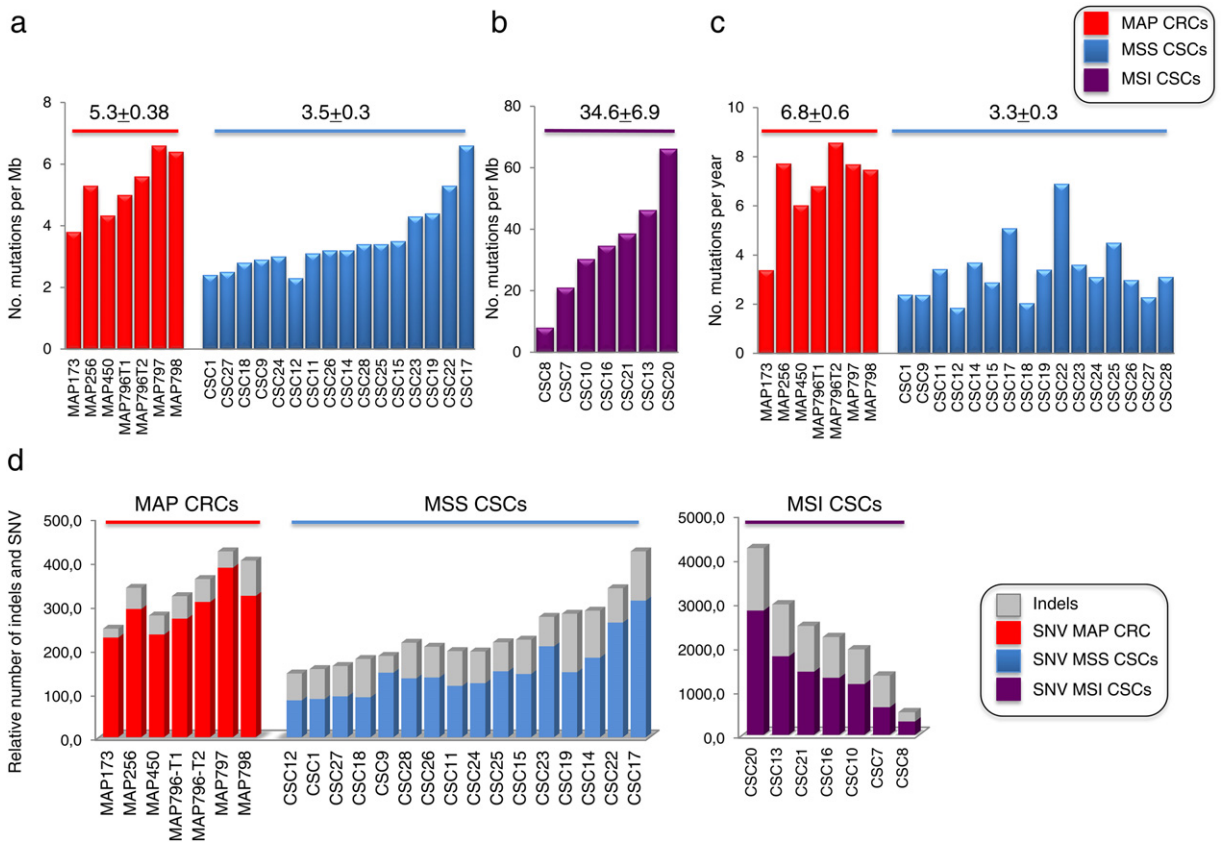

Fig. 1. Somatic mutation frequencies in MAP CRCs and colorectal CSCs. a) and b) Mutation frequencies per Mb in MAP CRCs (red), and MSS (blue) and MSI CSCs (purple). c) Mutation rates in MAP CRCs and MSS CSCs calculated by dividing the number of somatic mutations per tumour by the age of the patient at diagnosis. d) Distribution of indels (grey) and SNVs in MAP CRCs (red), and MSS (blue) and MSI (purple) CSCs. Data are mean ± SE.

not a characteristic of MAP CRCs and there were no detectable alterations of microsatellite markers (*NR21*, *BAT-26*, *BAT-25*, *NR-24*, *MONO-27*) (Fig. S1).

MAP CRCs exhibited a homogeneous mutational spectrum in the seven patients, which was characterized by the prevalence of two mutational classes, G:C>T:A transversions and G:C>A:T transitions (Fig. 2A).

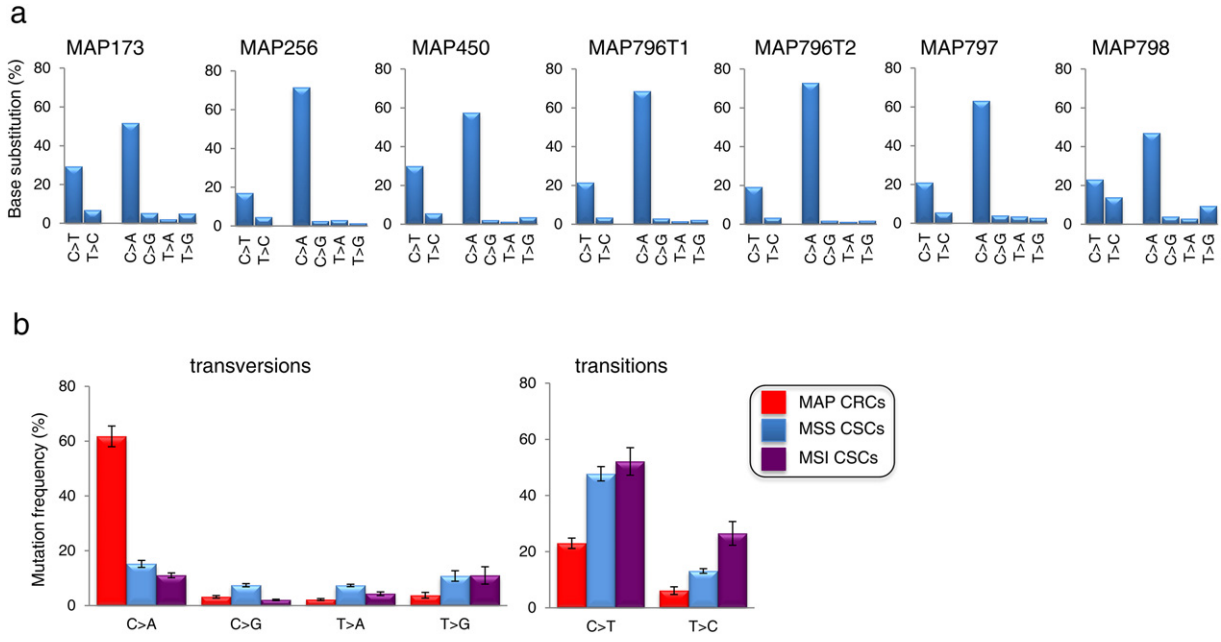

Fig. 2. Mutational spectra in MAP CRCs and colorectal CSCs. a) Mutational spectrum for base substitutions in each MAP CRC. b) Comparison of average values of transitions and transversions in MAP CRCs (red), MSS CSCs (blue) and MSI CSCs (purple). Data are mean ± SE. Each class of mutation in MAP CRC was statistically significant different from MSS and MSI CSCs with *P* values < 0.001 (Student's *t*-test).

By comparison with MSS and MSI CSCs, there was a significant overrepresentation of G:C>T:A in MAP CRC, with all the other mutational classes occurring at decreased frequencies (Fig. 2B). The transversions were equally distributed between coding and non-coding strands (1.01 ratio). Taken together, these findings are fully consistent with mutation induction by persistent DNA 8-oxoG:A mismatches resulting from the *MUTYH* defect.

3.2. Fingerprint of Base Substitutions in MAP CRCs

To identify the mutational signature associated with persistent 8-oxoG:A mispairs, we performed a refined classification of base substitutions to include the 3′ and 5′ flanking bases at the mutated site (Alexandrov et al., 2013a,b). This identified a strongly conserved MAP signature, mostly characterized by biases among the possible positions of C>A and C>T base substitutions (substitutions in mutational signatures are referred to by the pyrimidine of the mutated Watson–Crick base pair; Fig. 3). It is noteworthy that identical SNVs distributions occurred in tumours from the distal and proximal colon of MAP796 patient (T1 and T2 in the sigmoid and caecum, respectively) indicating that these tumours have a common molecular origin (Fig. 3).

To determine whether the mutational profiles of MAP CRCs differed from those observed in CSCs we applied principal component analysis (PCA). This revealed a perfect separation between the signatures of

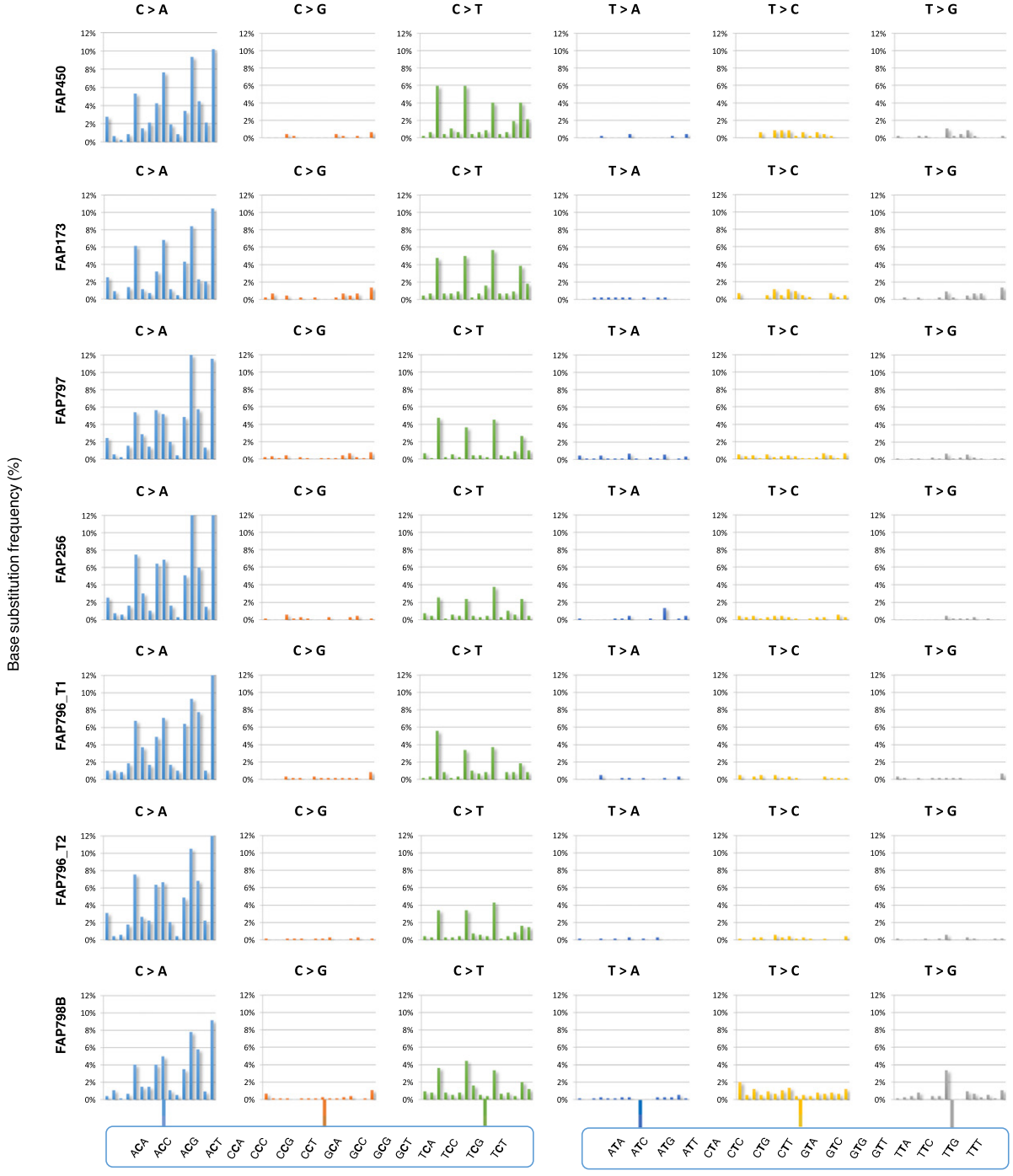

Fig. 3. Fingerprints of transitions and transversions in MAP CRCs. Mutational signatures are defined by the substitution class (in different colours) and the sequence context immediately 5′ and 3′ to the mutated base. The mutation types are on the horizontal axes, whereas vertical axes show the recurrence of mutations occurring in the specific sequence context.

MAP and CSCs (Fig. 4A and Table S2). The signatures endowed with the greater discriminant power for this separation were C>A transversions at 5′-T**C**T-3′, 5′-T**C**A-3′ and, to a lower extent, 5′-G**C**A-3′, 5′-C**C**A-3′, 5′-T**C**C-3′, 5′-G**C**T-3′ and 5′-C**C**T-3′ trinucleotides (Fig. 4B). All these signatures identify sequences where the damaged base (8-oxoG) is assumed to be the complementary guanine in the C:G pair.

Trinucleotide signatures from MAP CRCs and CSCs were compared to a catalogue of known mutational signatures identified from >12,000 samples derived from 40 types of human cancer (Alexandrov et al., 2013a,b). The frequently observed Signatures 1 and 5 were also present in MAP and CSCs (Fig. 4C and D) (Alexandrov et al., 2013a). In addition, fingerprints associated with MMR-defective CSCs corresponded to signatures 6, 15 and 26 that are typical of MSI tumours and a signature of unknown origin, Signature 17, was also present in three CSCs. MAP CRCs were characterized by a novel signature, termed Signature 36, which is almost exclusively defined by the specific locations of G:C>T:A transversions (Fig. 4C and D). Signature 36 identifies the location at which mutations arise because of unrepaired 8-oxoG:A mispairs and is essentially identical (correlation 0.98) to that reported for germline mutations occurring in *Mutyh*/*Ogg1*/*Mth1* triple knock-out mice (Ohno et al., 2014) (Fig. 4D). This suggests that the unique spectrum of mutations in MAP tumours mainly reflects MUTYH loss and the sequence specificity of DNA 8-oxoG formation.

3.3. Identification of Oncogenes/Tumour Suppressors Specifically Associated with MAP CRC

It has been proposed that carcinogenesis in *MUTYH*-associated polyposis follows a distinct genetic pathway (Lipton et al., 2003). Recurrently mutated genes in 7 MAP CRCs were identified using MuTect and manual curation (Fig. 5A). These included *APC*, *KRAS*, *PIK3CA*, *FAT4*, *TP53*, *FAT1*, *AMER1* (*or WTX*), *KDM6A*, *SMAD4* and *SMAD2* (a more complete list of genes and detailed mutation analysis are reported in Tables S3 and S4). Targeted exome sequencing of 10 additional MAP CRCs (Table S5) confirmed the MAP-related mutagenic profiles of these 10 genes (Fig. 5B).

To examine whether these mutations were present at the adenoma stage, targeted sequencing was performed in 26 MAP adenomas (Fig. 5C and Table S5). *AMER1* and *APC* were equally mutated in adenomas and CRCs consistent with early occurrence and confirming their role as driver genes in MAP (Rashid et al., 2016). In contrast *SMAD2*, *SMAD4* and *TP53* were rarely mutated in adenomas indicating that they represent late events in colorectal carcinogenesis. It was not possible to assign early or late occurrence to the other five genes.

Comparison of MAP mutations to 376 MMR-proficient and -deficient CRCs in COSMIC identified three different patterns of putative driver mutations (Fig. 5D). *KRAS*, *SMAD4*, *SMAD2* and *KDM6A*

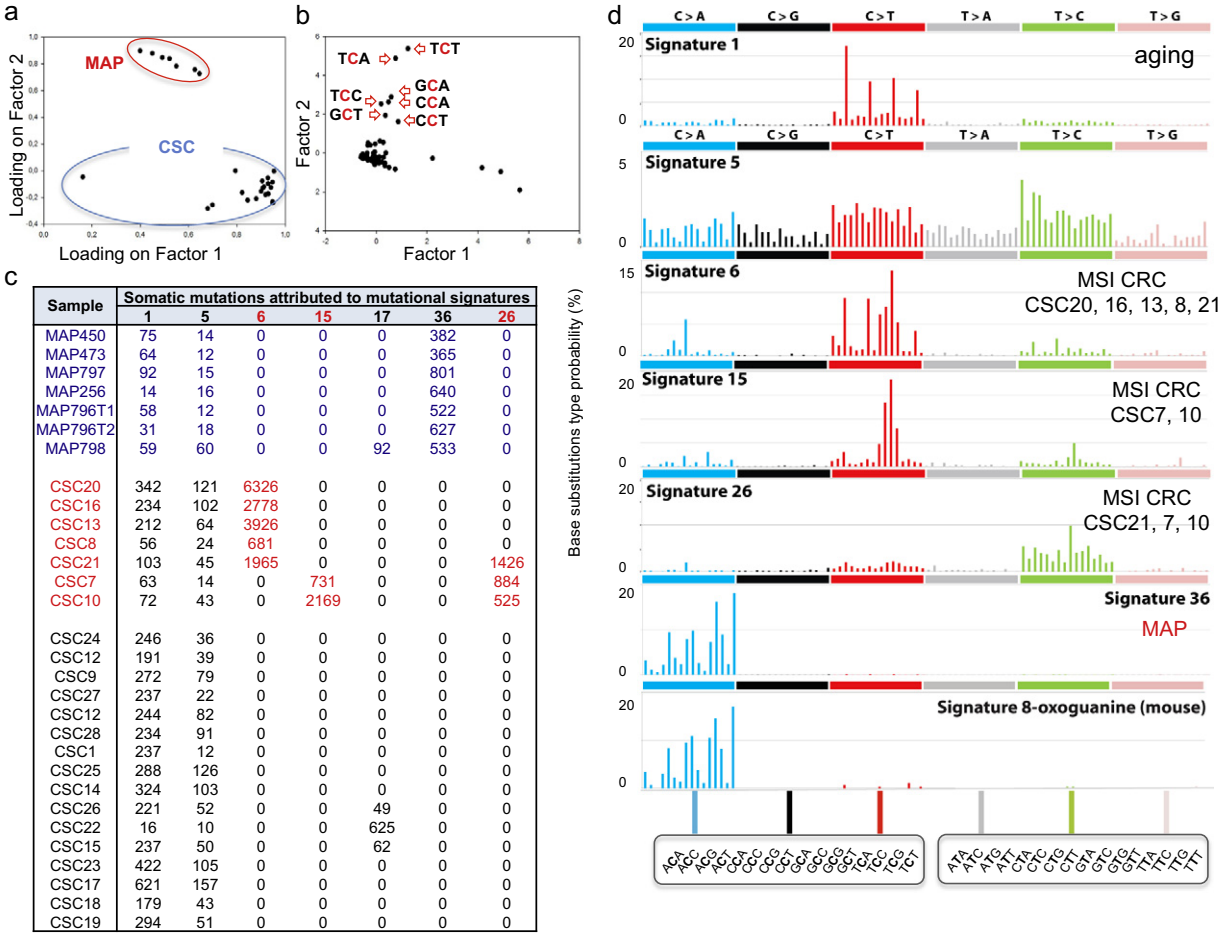

Sample	Somatic mutations attributed to mutational signatures						
	1	5	6	15	17	36	26
MAP450	75	14	0	0	0	382	0
MAP473	64	12	0	0	0	365	0
MAP797	92	15	0	0	0	801	0
MAP256	14	16	0	0	0	640	0
MAP796T1	58	12	0	0	0	522	0
MAP796T2	31	18	0	0	0	627	0
MAP798	59	60	0	0	92	533	0
CSC20	342	121	6326	0	0	0	0
CSC16	234	102	2778	0	0	0	0
CSC13	212	64	3926	0	0	0	0
CSC8	56	24	681	0	0	0	0
CSC21	103	45	1965	0	0	0	1426
CSC7	63	14	0	731	0	0	884
CSC10	72	43	0	2169	0	0	525
CSC24	246	36	0	0	0	0	0
CSC12	191	39	0	0	0	0	0
CSC9	272	79	0	0	0	0	0
CSC27	237	22	0	0	0	0	0
CSC12	244	82	0	0	0	0	0
CSC28	234	91	0	0	0	0	0
CSC1	237	12	0	0	0	0	0
CSC25	288	126	0	0	0	0	0
CSC14	324	103	0	0	0	0	0
CSC26	221	52	0	0	49	0	0
CSC22	16	10	0	0	625	0	0
CSC15	237	50	0	0	62	0	0
CSC23	422	105	0	0	0	0	0
CSC17	621	157	0	0	0	0	0
CSC18	179	43	0	0	0	0	0
CSC19	294	51	0	0	0	0	0

Fig. 4. Mutational signatures in MAP CRCs and MSS and MSI CSCs. a) Separation between MAP (red) and CSCs (blue) mutational fingerprints by PCA. Factor 1 and Factor 2 represent commonality and differences among profiles, respectively. b) G:C>T:A transversions at the indicated trinucleotides identify signatures with the greater discriminant power for MAP/CSCs separation. c) Somatic mutations in MAP CRCs (red) and MSI/MSS CSCs (black) attributed to reported mutational signatures (Alexandrov et al., 2013a,b). d) Graphical representations of signatures identified in MSI/MSS CSCs and MAP CRCs. Signature 8-oxoguanine derives from mice defective in *Mutyh*/*Ogg1*/*Mth1* (Ohno et al., 2014).

were preferentially mutated in MAP compared to MSS and MSI CRCs. A second group of genes (*FAT4*, *FAT1 AMER1* and *PIK3CA*) were mutated at similar frequencies in MAP and MSI CRCs. *APC* and *TP53* comprised a third group that was equally mutated in all CRCs.

Thus, alterations in MAP CRCs affect the well-established *WNT*, *TGFβ*, *PI3K*, *RAS* and *p53* signalling pathways (Cancer Genome Atlas Network, 2012). The mutational profiles also reveal the specificity of MAP oncogenesis, with limited features in common with MMR-proficient and -deficient CRC.

3.4. Mutational Signature in Oncogenes/Tumour Suppressors

The identified trinucleotide mutational signature for G:C>T:A transversions was also present in recognized target genes for MAP (Al-Tassan et al., 2002; Jones et al., 2002, 2004). An excess of G:C>T:A transversions in *APC* leading to protein truncation has been reported (Al-Tassan et al., 2002; Sieber et al., 2003; Jones et al., 2002). Besides confirming this observation (G:C>T:A were 23/32, >70% of the identified *APC* variants), we noticed that these transversions occurred almost exclusively in the identified "hot-spots" for 8-oxoG (Table 1). Similarly the majority of SNV in the *AMER1* driver gene were also G:C>T:A transversions (14/24, 58% of total mutations) in the first base of GAG and GAA codons that lead to the formation of TAG and TAA stop codons. Analysis of the 5′ and 3′ flanking bases at the mutated site confirmed that these mutations are also within the recognized trinucleotide signature (i.e. Signature 36) for 8-oxoG (Table 1).

Missense G:C>T:A transversions were also preferentially located in identified "hot-spots" of DNA oxidation in other key genes for MAP (*PIK3CA*, *SMAD4 and SMAD2)* (Table S6). This was true even if the frequency of the transversions was lower than expected (35–20% in *TP53*, *FAT1*, *FAT4*) (Table S7).

KRAS mutations in MAP CRCs exhibited a distinctive pattern of mutations. They were exclusively G:C>T:A transversions at the 1st G of codon 12 (**G**GT>**T**GT, nt 34) to generate a MAP-specific G12C variant (Jones et al., 2002, 2004; Venesio et al., 2013). This is in contrast to sporadic CRCs in which G:C>T:A transversions predominantly affect the 2nd G of the same codon (G**G**T>G**T**T, nt 35) leading to the G12V variant (Fig. 6A) (Cox et al., 2014). Indeed **G** preceded by a T in 5′-T**G***G-3′ is a

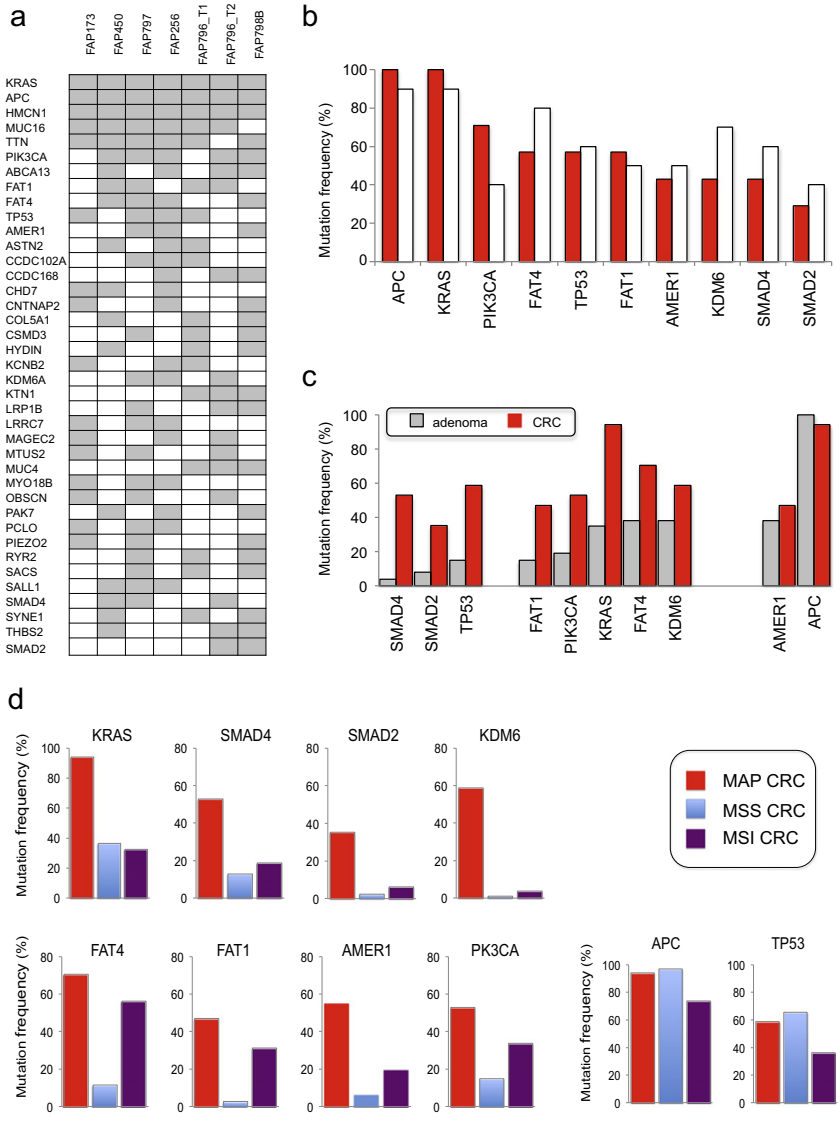

Fig. 5. Mutation analysis of target genes in CRCs and adenomas of MAP patients. a) Genes mutated in 7 MAP CRCs and identified by exome sequencing. Only genes mutated in ≥2 patients are shown. b) Comparison of the mutation frequency in 7 MAP CRCs analyzed by WES (red) and 10 CRCs analyzed by targeted sequencing (open bars) from independent MAP patients. c) Comparison of mutation frequency of the indicated genes in 26 adenomas (grey) and 17 CRCs (red) from MAP patients. d) Comparison of mutation frequency in the indicated genes in MAP CRCs (red), and MSS (blue) and MSI (purple) CRCs (data from a database of 376 samples).

mutational "hot-spot" in MAP CRCs, whereas G preceded by G in 5′-G**G***T-3′ is a "cold-spot" (Fig. 6B). To examine whether this mutational bias reflected the sequence dependence of DNA 8-oxoG formation or the particularly efficient processing of 8-oxoG at nt 34 by active MUTYH, we examined the activity of purified MUTYH on duplexes containing a single 8-oxoG:A basepair located at nt 34 or at nt 35 of the *KRAS* sequence (Fig. 6A). We did not observe any difference in MUTYH processing of these two substrates (Fig. 6B,C) and we conclude that the overrepresentation of the G12C mutations in MAP CRC reflects the particular susceptibility of G34 to oxidation. Thus, the different probabilities of ROS-mediated guanine oxidation are likely to be a significant determinant in the mutational signature in MAP CRCs.

4. Discussion

Our analysis of cancer-related mutations associated with *MUTYH* inactivation in MAP reveals that the absence of MUTYH-mediated processing of 8-oxoG:A mispairs results in a relatively modest mutator phenotype. The increase in mutation rates in MAP CRC is similar to that in lymphoblastoid cell lines established from MAP patients (1.5- to 4.0-fold) (Ruggieri et al., 2013; Grasso et al., 2014). It therefore appears that even a small increase in mutation rate due to impaired repair of pre-mutagenic oxidative DNA lesions is an important risk factor for cancer. CRC is the main cancer in MAP. It occurs with a relatively early age of onset (47 years in our MAP cases) and a lifetime risk approaching 100% (Nielsen et al., 2010). It is noteworthy that MUTYH-defective cells are hypermutable by oxidants, indicating that the mild mutator phenotype can be significantly enhanced under oxidative stress conditions (Ruggieri et al., 2013; Grasso et al., 2014). Recently a correlation has been drawn between the lifetime risk of cancer and the total number of cell divisions in a given tissue (Tomasetti and Vogelstein, 2015). Based on the present observations we propose that a combination of endogenous and exogenous oxidation sources (environmental factors) and lack of DNA repair (inherited predisposition) acting on a highly self-renewing tissue are the main determinants of the increased MAP cancer susceptibility.

Detailed analysis of MAP CRC mutations revealed a substantial increase in a single class of base substitutions, G:C>T:A transversions. This is in accordance with the expected persistence of DNA 8-oxoG:A mismatches, the preferred MUTYH substrate. MUTYH also removes 2-hydroxyadenine from 2-hydroxyadenine: G mispairs (Ohtsubo et al., 2015). If unrepaired, these generate A:T>C:G transversions (Satou et al., 2007). We did not observe increase in this class of mutations in MAP CRCs and it appears that oxidation of DNA adenine is most likely a relatively infrequent occurrence. Mutations associated with the miscoding properties of DNA 8-oxoG are therefore the hallmark of MUTYH inactivation.

The MAP CRC G:C>T:A transversions were equally distributed in the transcribed and non-transcribed strands. This is at variance with the strong bias towards higher rates of G:C>T:A transversions located in the non-transcribed strand in cutaneous squamous cell carcinoma and UV-irradiated normal human skin (Martincorena et al., 2015). The lack of transcriptional strand bias is a strong indicator that 8-oxoG:A mismatches are not processed by transcription-coupled BER in the colon.

More importantly, analysis of the sequence context of the G:C>T:A transversions identified a specific mutational signature due to unrepaired DNA 8-oxoG (Signature 36). It is particularly significant that Signature 36 is almost identical to the signature of spontaneous mutations in *Ogg1*$^{-/-}$, *Mutyh*$^{-/-}$, *Mth1*$^{-/-}$ mice in which all known repair systems for DNA 8-oxoG are disabled (Ohno et al., 2014). These coincident signatures indicate that MUTYH plays the leading role in protecting the human genome against mutations induced by DNA 8-oxoG.

The types and location of mutations in oncogene/tumour suppressor genes also implicate DNA 8-oxoG in MAP CRC development. KRAS activation provides the best example of this. 100% of *KRAS* mutations are codon 12 G:C>T:A transversions that correspond to the acknowledged preferential oxidation of 5′-G of GG and GGG sequences under oxidative

Table 1
Location of G:C>T:A transversions in the *APC* and *AMER1* genes.[a]

APC G:C>T:A 23/32 (71.8%)

Tumour	Aa change	Sequence context[b]	Trinucleotide[c]
MAP104T1	E225*	CGAA>CTAA	CGA:TCG
MAP356T2	S688*	TCA>TAA	TGA:TCA
	E1306*	AGAA>ATAA	AGA:TCT
MAP443T1	E763*	AGAA>ATAA	AGA:TCT
	E1408*	TGAA>TTAA	TGA:TCA
MAP256	E850*	AGAA>ATAA	AGA:TCT
	E1558*	AGAA>ATAA	AGA:TCT
MAP873T1	E902*	GGAA>GTAA	GGA:TCC
	E1374*	TGAA>TTAA	TGA:TCA
MAP450	E923*	GGAA/GTAA	GGA:TCC
	E1390*	TGAA>TTAA	TGA:TCA
MAP356T1	E1136*	TGAA>TTAA	TGA:TCA
	R2565I	AGA>ATA	AGA:TCT
MAP797	S1258*	TCA>TAA	TGA:TCA
	E1536*	AGAA>ATAA	AGA:TCT
MAP902T1	S1282*	TCA>TAA	TGA:TCA
MAP901T1	E1284*	TGAA>TTAA	TGA:TCA
MAP173	E1379*	GGAG>GTAG	GGA:TCC
MAP796T1	E1379*	GGAG>GTAG	GGA:TCC
	E1542*	TGAA>TTAA	TGA:TCA
MAP897T1	S1392*	TCA>TAA	TGA:TCA
MAP798	E1544*	AGAA>ATAA	AGA:TCT
MAP896T1	S1567*	TCA>TAA	TGA:TCA

AMER1 G:C>T:A 14/24 (58.3%)

Tumour	Aa change	Sequence context[b]	Trinucleotide[c]
MAP422T1	E 334*	AGAA>ATAA	AGA:TCT
MAP797	E386*	AGAA>ATAA	AGA:TCT
MAP256	E386*	AGAA>ATAA	AGA:TCT
MAP483T2	E386*	AGAA>ATAA	AGA:TCT
MAP577T2	E394*	AGAA>ATAA	AGA:TCT
MAP897T1	E394*	AGAA>ATAA	AGA:TCT
MAP677T1	E395*	TGAG>TTAG	TGA:TCA
MAP181T2	E407*	AGAA>ATAA	AGA:TCT
MAP181T6	E462*	AGAA>ATAA	AGA:TCT
MAP901T1	E469*	TGAA>TTAA	TGA:TCA
MAP577T1	E480*	TGAG>TTAG	TGA:TCA
MAP483T4	E485*	TGAG>TTAG	TGA:TCA
MAP798	E587*	AGAA>ATAA	AGA:TCT
MAP356T1	D753Y	AGAT>ATAT	AGA:TCT

[a] The sequence context of G:C>T:A transversions inAPC is shown only in CRCs and in both adenomas and CRCs (bolded) inAMER1.
[b] Codons are shown in red and the mutated base is underlined.
[c] "Hot-spot" and "cold-spot" trinucleotides are respectively in red and black.

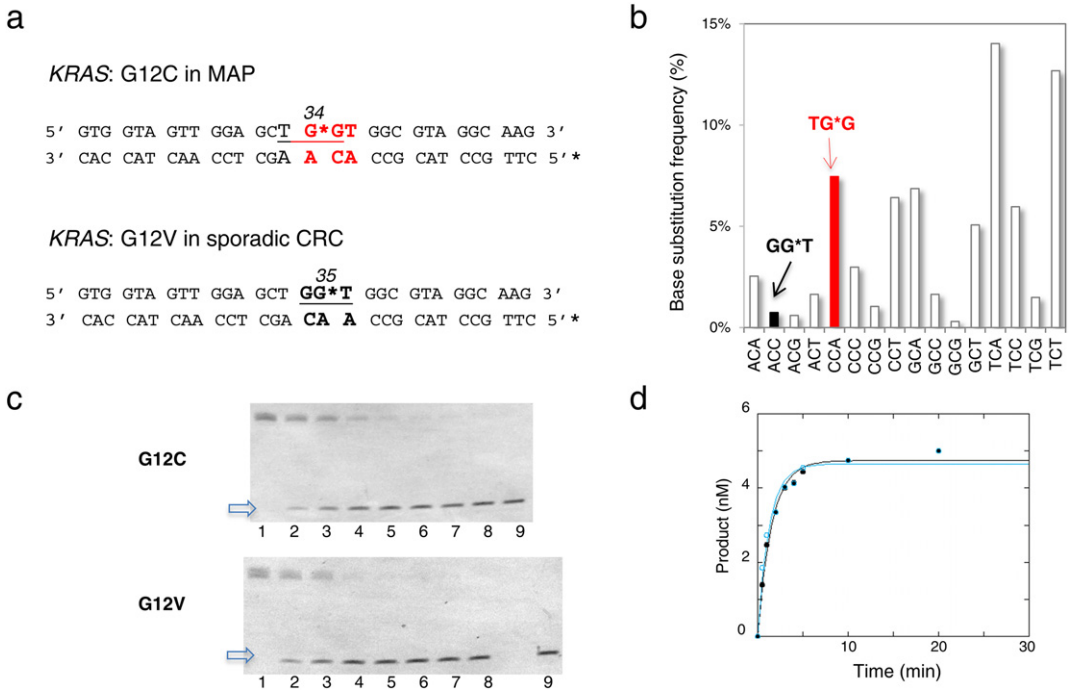

Fig. 6. *KRAS* sequence context and MUTYH adenine glycosylase activity. a) Duplex oligonucleotides containing a single 8-oxoG:A mispair at nt 34 or 35 of the *KRAS* sequence which are responsible for the G12C and G12V variants in MAP (top) and sporadic CRC (bottom). Codon 12 is in bold and trinucleotides containing 8-oxoG (G*) are underlined. b) Base substitution frequency of C>A transversions in MAP CRC. The black and red bars represent the GG*T "cold-spot" and TG*G "hot-spot" trinucleotides, respectively. c) Representative gels of single-turnover MUTYH assays using duplexes shown in panel A. DNA glycosylase activity of human MUTYH on single 8-oxoG:A mispairs was assayed using 10 nM duplex substrates and 20 nM active protein. Reaction products are indicated by an arrow. Lanes 1–9: 0, 0.5, 1, 2, 3, 4, 5, 10 and 20 min. d) Plots of MUTYH glycosylase assay data under single-turnover conditions. Data were derived from image analysis of gels by *Image J* and *Kaleidagraph* softwares. Values are the average from two independent experiments. G12C sequence (full black circle); G12 V (empty blue circle).

stress conditions (Kawanishi et al., 2001). This sequence preference gives rise to the G12C variant that predominates in MAP CRC rather than the G12D or G12 V mutations that are common in sporadic CRCs (Cox et al., 2014). It is noteworthy that G12C is the most frequent *KRAS* mutation in non-small-cell lung cancers in which an excess of G:C>T:A transversions may be the result of oxidative DNA damage associated with exposure to tobacco smoke (Govindan et al., 2012).

Mutations in other "driver" genes of colorectal carcinogenesis such as *APC* and *AMER1* also showed the 8-oxoG-dependent sequence context specificity. In this case mutations occurred mainly at AGA and TGA sites. Thus similarly to the 5′-GG-3′ *KRAS* hot-spot, the G in GA dinucleotides is also easily oxidized. The preferential oxidation of G in GA or GG is consistent with a reduced ionization potential of these purine dinucleotides. Base type, orientation and stacking interaction of consecutive bases are the main determinants of the ionization potential (Sugiyama and Saito, 1996). The majority of mutations in both *APC* and *AMER1* were G:C > T:A transversions generating stop codons. Interestingly the relatively rare *AMER1* mutations in sporadic CRC (10%) show a wider spectrum of molecular changes including stop gain, missense, and synonymous variants (Sanz-Pamplona et al., 2015). Our data suggest that the accumulation of sequence specific 8-oxoG:A mispairs due to *MUTYH* inactivation is the cause of the increased mutability of this gene and the strong drift towards stop codon formation. The observation that a specific 8-oxoG mutational fingerprint increases the probability of mutating specific oncogenes/tumour suppressors is a rule confirmed in several examples (such as *PIK3CA*, *SMAD4*, *SMAD2*, *TP53*, *FAT4* and *FAT1*). Although the pathways involved in MAP CRC are the *WNT*, *TGFβ*, *PI3K*, *RAS* and *p53* signalling pathways (Cancer Genome Atlas Network, 2012), which are commonly mutated in sporadic CRC, the MUTYH defect directs oncogenesis towards specific genes that are mutated less frequently in sporadic CRCs. In this sense the consequence of MUTYH inactivation resembles that of MMR loss. In both cases mutation of oncogenes/tumour suppressors is driven by the mutator phenotype that affects sequence specific structural elements, although with clearly different molecular outcomes (transversions versus frame-shift mutations).

The accumulation of mutations in DNA coding regions of MAP CRCs might translate into an excess of neoepitopes able to trigger an anti-tumour immune response. Similarly to the MMR-defective cancers, the high antigenic potential of these tumours could be associated with the improved clinical outcome reported for MAP patients (Nielsen et al., 2010). Therefore, it would be interesting to explore if the missense mutations we have identified in the target genes might have immunogenic properties.

In conclusion, by exomic sequencing of CRCs from MAP patients we have identified a novel mutational signature (Signature 36) that results from the failure to repair a specific product of DNA oxidation and is associated with an increased risk of cancer. It is remarkable that the MAP-specific Signature 36 has never been identified in sporadic CRC. This suggests that mutations due to unrepaired DNA 8-oxoG:A mispairs are confined to MAP CRCs. We note, however, that Signature 36 closely resembles Signature 18 (Pearson correlation coefficient of 0.77) that is particularly prevalent in neuroblastoma in which it comprises >50% of mutations (Fig. S2). Signature 18 has also been found at lower levels in pancreas, breast, and gastric cancers. It is possible therefore that oxidative DNA damage also contributes to cancer aetiology in these organs.

Supplementary data to this article can be found online at http://dx.doi.org/10.1016/j.ebiom.2017.04.022.

Conflict of Interest

None.

Author Contributions

MB and AV designed the study. AB, EM and MT analyzed and interpreted whole-exome sequencing data. AV and RM collected and prepared tumour samples and analyzed targeted sequencing data. VC, MGD, MF and EDU collected tumour samples and interpreted histology. MG, ELC, MQ, AM, MA and TV performed genetic testing and somatic mutation analyses. MG, ELC, LSM and VS were responsible for patient counselling and clinical data acquisition. FM and FG performed MUTYH enzymatic assays. EP and MBa provided a molecular characterization of CSCs. GG provided technical support and conceptual advice. LBA constructed mutational fingerprints and interpreted sequencing data. MB and MT jointly supervised this work. MB, EM and AV wrote the manuscript, with assistance and final approval from all co-authors.

Acknowledgements

We thank Peter Karran and Eugenia Dogliotti for critical reading of the manuscript. This work was supported by research grants to MB, FM and MT from the Associazione Italiana Ricerca sul Cancro (IG grants 11755 and 17583, and "5x1000" grant 9979) and MB, FM and AV from the Italian Ministry of Health (Grant RF-2008) (Project "Malattie Rare"). LBA is personally supported through a J. Robert Oppenheimer Fellowship at Los Alamos National Laboratory. This research used resources provided by the Los Alamos National Laboratory Institutional Computing Program, which is supported by the U.S. Department of Energy National Nuclear Security Administration under Contract No. DE-AC52-06NA25396. Research performed at Los Alamos National Laboratory was carried out under the auspices of the National Nuclear Security Administration of the United States Department of Energy.

References

Alexandrov, L.B., 2015. Understanding the origins of human cancer. Science 350, 1175.
Alexandrov, L.B., Nik-Zainal, S., Wedge, D.C., Campbell, P.J., Stratton, M.R., 2013a. Deciphering signatures of mutational processes operative in human cancer. Cell Rep. 3, 246–259.
Alexandrov, L.B., Nik-Zainal, S., Wedge, D.C., Aparicio, S.A., Behjati, S., Biankin, A.V., Bignell, G.R., Bolli, N., Borg, A., Børresen-Dale, A.L., et al., 2013b. Signatures of mutational processes in human cancer. Nature 500, 415–421.
Alexandrov, L.B., Jones, P.H., Wedge, D.C., Sale, J.E., Campbell, P.J., Nik-Zainal, S., Stratton, M.R., 2015. Clock-like mutational processes in human somatic cells. Nat. Genet. 47, 1402–1407.
Al-Tassan, N., Chmiel, N.H., Maynard, J., Fleming, N., Livingston, A.L., Williams, G.T., Hodges, A.K., Davies, D.R., David, S.S., Sampson, J.R., et al., 2002. Inherited variants of MYH associated with somatic G:C>T:A mutations in colorectal tumors. Nat. Genet. 30, 227–232.
Aretz, S., Tricarico, R., Papi, L., Spier, I., Pin, E., Horpaopan, S., Cordisco, E.L., Pedroni, M., Stienen, D., Gentile, A., et al., 2014. MUTYH-associated polyposis (MAP): evidence for the origin of the common European mutations p.Tyr179Cys and p.Gly396Asp by founder events. Eur. J. Hum. Genet. 22, 923–929.
Cox, A.D., Fesik, S.W., Kimmelman, A.C., Luo, J., Der, C.J., 2014. Drugging the undruggable RAS: mission possible? Nat. Rev. Drug Discov. 13, 828–851.
D'Agostino, V.G., Minoprio, A., Torreri, P., Marinoni, I., Bossa, C., Petrucci, T.C., Albertini, A.M., Ranzani, G.N., Bignami, M., Mazzei, F., 2010. Functional analysis of MUTYH mutated proteins associated with familial adenomatous polyposis. DNA Repair (Amst) 9, 700–707.
De Angelis, M.L., Zeuner, A., Policicchio, E., Russo, G., Bruselles, A., Signore, M., Vitale, S., De Luca, G., Pilozzi, E., Boe, A., et al., 2016. Cancer stem Cell-based models of colorectal cancer reveal molecular determinants of therapy resistance. Stem Cells Transl. Med. 5, 511–523.
Govindan, R., Ding, L., Griffith, M., Subramanian, J., Dees, N.D., Kanchi, K.L., Maher, C.A., Fulton, R., Fulton, L., Wallis, J., et al., 2012. Genomic landscape of non-small cell lung cancer in smokers and never-smokers. Cell 150, 1121–1134.
Grasso, F., Giacomini, E., Sanchez, M., Degan, P., Gismondi, V., Mazzei, F., Varesco, L., Viel, A., Bignami, M., 2014. Genetic instability in lymphoblastoid cell lines expressing biallelic and monoallelic variants in the human MUTYH gene. Hum. Mol. Genet. 233, 843–852.
Helleday, T., Eshtad, S., Nik-Zainal, S., 2014. Mechanisms underlying mutational signatures in human cancers. Nat. Rev. Genet. 15, 585–598.
Hirano, S., Tominaga, Y., Ichinoe, A., Ushijima, Y., Tsuchimoto, D., Honda-Ohnishi, Y., Ohtsubo, T., Sakumi, K., Nakabeppu, Y., 2003. Mutator phenotype of MUTYH-null mouse embryonic stem cells. J. Biol. Chem. 278, 38121–38124.
Jones, S., Emmerson, P., Maynard, J., Best, J.M., Jordan, S., Williams, G.T., Sampson, J.R., Cheadle, J.P., 2002. Biallelic germline mutations in MYH predispose to multiple colorectal adenoma and somatic G:C–>T:A mutations. Hum. Mol. Genet. 11, 2961–2967.
Jones, S., Lambert, S., Williams, G.T., Best, J.M., Sampson, J.R., Cheadle, J.P., 2004. Increased frequency of the k-ras G12C mutation in MYH polyposis colorectal adenomas. Br. J. Cancer 90, 1591–1593.
Kawanishi, S., Hiraku, Y., Oikawa, S., 2001. Mechanism of guanine-specific DNA damage by oxidative stress and its role in carcinogenesis and aging. Mutat. Res. 488, 65–76.
Klungland, A., Rosewell, I., Hollenbach, S., Larsen, E., Daly, G., Epe, B., Seeberg, E., Lindahl, T., Barnes, D.E., 1999. Accumulation of premutagenic DNA lesions in mice defective in removal of oxidative base damage. Proc. Natl. Acad. Sci. U. S. A. 96, 13300–13305.
Lipton, L., Halford, S.E., Johnson, V., Novelli, M.R., Jones, A., Cummings, C., Barclay, E., Sieber, O., Sadat, A., Bisgaard, M.L., et al., 2003. Carcinogenesis in MYH-associated polyposis follows a distinct genetic pathway. Cancer Res. 63, 7595–7599.
Lynch, H.T., Snyder, C.L., Shaw, T.G., Heinen, C.D., Hitchins, M.P., 2015. Milestones of Lynch syndrome: 1895-2015. Nat. Rev. Cancer 15, 181–194.
Markkanen, E., Dorn, J., Hübscher, U., 2013. MUTYH DNA glycosylase: the rationale for removing undamaged bases from the DNA. Front. Genet. 4:18. http://dx.doi.org/10.3389/fgene.2013.00018.
Martincorena, I., Roshan, A., Gerstung, M., Ellis, P., Van Loo, P., McLaren, S., Wedge, D.C., Fullam, A., Alexandrov, L.B., Tubio, J.M., et al., 2015. Tumor evolution. High burden and pervasive positive selection of somatic mutations in normal human skin. Science 348, 880–886.
Mazzei, F., Viel, A., Bignami, M., 2013. Role of MUTYH in human cancer. Mutat. Res. 743–744, 33–43.
Mo, J.Y., Maki, H., Sekiguchi, M., 1992. Hydrolytic elimination of a mutagenic nucleotide, 8-oxodGTP, by human 18-kilodalton protein: sanitization of nucleotide pool. Proc. Natl. Acad. Sci. U. S. A. 89, 11021–11025.
Molatore, S., Russo, M.T., D'Agostino, V.G., Barone, F., Matsumoto, Y., Albertini, A.M., Minoprio, A., Degan, P., Mazzei, F., Bignami, M., et al., 2010. MUTYH mutations associated with familial adenomatous polyposis: functional characterization by a mammalian cell-based assay. Hum. Mutat. 31, 159–166.
Cancer Genome Atlas Network, 2012. Comprehensive molecular characterization of human colon and rectal cancer. Nature 487, 330–337.
Nielsen, M., van Steenbergen, L.N., Jones, N., Vogt, S., Vasen, H.F., Morreau, H., Aretz, S., Sampson, J.R., Dekkers, O.M., Janssen-Heijnen, M.L., et al., 2010. Survival of MUTYH-associated polyposis patients with colorectal cancer and matched control colorectal cancer patients. J. Natl. Cancer Inst. 102, 1724–1730.
Ohno, M., Sakumi, K., Fukumura, R., Furuichi, M., Iwasaki, Y., Hokama, M., Ikemura, T., Tsuzuki, T., Gondo, Y., Nakabeppu, Y., 2014. 8-oxoguanine causes spontaneous de novo germline mutations in mice. Sci. Rep. 4, 4689.
Ohtsubo, T., Nishioka, K., Imaiso, Y., Iwai, S., Shimokawa, H., Oda, H., Fujiwara, T., Nakabeppu, Y., 2015. Identification of human MutY homolog (hMYH) as a repair enzyme for 2-hydroxyadenine in DNA and detection of multiple forms of hMYH located in nuclei and mitochondria. Nucleic Acids Res. 43, 3870–3871.
Palles, C., Cazier, J.B., Howarth, K.M., Domingo, E., Jones, A.M., Broderick, P., Kemp, Z., Spain, S.L., Guarino, E., Salguero, I., et al., 2013. Germline mutations affecting the proofreading domains of POLE and POLD1 predispose to colorectal adenomas and carcinomas. Nat. Genet. 45, 136–144.
Rashid, M., Fischer, A., Wilson, C.H., Tiffen, J., Rust, A.G., Stevens, P., Idziaszczyk, S., Maynard, J., Williams, G.T., Mustonen, V., et al., 2016. Adenoma development in familial adenomatous polyposis and MUTYH-associated polyposis: somatic landscape and driver genes. J. Pathol. 238, 98–108.
Ricci, M.T., Miccoli, S., Turchetti, D., Bondavalli, D., Viel, A., Quaia, M., Giacomini, E., Gismondi, V., Sanchez-Mete, L., Stigliano, V., et al., 2017. Type and frequency of MUTYH variants in Italian patients with suspected MAP: a retrospective multicenter study. J. Hum. Genet. 62, 309–315.
Ruggieri, V., Pin, E., Russo, M.T., Barone, F., Degan, P., Sanchez, M., Quaia, M., Minoprio, A., Turco, E., Mazzei, F., et al., 2013. Loss of MUTYH function in human cells leads to accumulation of oxidative damage and genetic instability. Oncogene 32, 4500–4508.
Sanz-Pamplona, R., Lopez-Doriga, A., Paré-Brunet, L., Lázaro, K., Bellido, F., Alonso, M.H., Aussó, S., Guinó, E., Beltrán, S., Castro-Giner, F., et al., 2015. Exome sequencing reveals AMER1 as a frequently mutated gene in colorectal cancer. Clin. Cancer Res. 21, 4709–4718.
Satou, K., Kasai, H., Masutani, C., Hanaoka, F., Harashima, H., Kamiya, H., 2007. 2-Hydroxy-2′-deoxyadenosine 5′-triphosphate enhances AT>CG mutations caused by 8-hydroxy-2′-deoxyguanosine 5′-triphosphate by suppressing its degradation upon replication in a HeLa extract. Biochemistry 46 (22), 6639–6646.
Schulze, K., Imbeaud, S., Letouzé, E., Alexandrov, L.B., Calderaro, J., Rebouissou, S., Couchy, G., Meiller, C., Shinde, J., Soysouvanh, F., et al., 2015. Exome sequencing of hepatocellular carcinomas identifies new mutational signatures and potential therapeutic targets. Nat. Genet. 47, 505–511.
Sieber, O.M., Lipton, L., Crabtree, M., Heinimann, K., Fidalgo, P., Phillips, R.K., Bisgaard, M.L., Orntoft, T.F., Aaltonen, L.A., Hodgson, S.V., et al., 2003. Multiple colorectal adenomas, classic adenomatous polyposis, and germ-line mutations in MYH. N. Engl. J. Med. 348, 791–799.
Sugiyama, H., Saito, I., 1996. Theoretical studies of GG-specific photocleavage of DNA via electron transfer: significant lowering of ionization potential and 5′-localization of HOMO of stacked GG bases in B-form DNA. J. Am. Chem. Soc. 118, 7063–7068.
Tomasetti, C., Vogelstein, B., 2015. Cancer etiology. Variation in cancer risk among tissues can be explained by the number of stem cell divisions. Science 347, 78–81.
Tomasetti, C., Marchionni, L., Nowak, M.A., Parmigiani, G., Vogelstein, B., 2015. Only three driver gene mutations are required for the development of lung and colorectal cancers. Proc. Natl. Acad. Sci. U. S. A. 112, 118–123.

Tsuzuki, T., Egashira, A., Igarashi, H., Iwakuma, T., Nakatsuru, Y., Tominaga, Y., Kawate, H., Nakao, K., Nakamura, K., Ide, F., et al., 2001. Spontaneous tumorigenesis in mice defective in the MTH1 gene encoding 8-oxo-dGTPase. Proc. Natl. Acad. Sci. U. S. A. 98, 11456–11461.

Tsuzuki, T., Nakatsu, Y., Nakabeppu, Y., 2007. Significance of error-avoiding mechanisms for oxidative DNA damage in carcinogenesis. Cancer Sci. 98, 465–470.

Turco, E., Ventura, I., Minoprio, A., Russo, M.T., Torreri, P., Degan, P., Molatore, S., Ranzani, G.N., Bignami, M., Mazzei, F., 2013. Understanding the role of the Q338H MUTYH variant in oxidative damage repair. Nucleic Acids Res. 41, 4093–4103.

Umar, A., Boland, C.R., Terdiman, J.P., Syngal, S., de la Chapelle, A., Rüschoff, J., Fishel, R., Lindor, N.M., Burgart, L.J., Hamelin, R., et al., 2004. Revised Bethesda Guidelines for hereditary nonpolyposis colorectal cancer (Lynch syndrome) and microsatellite instability. J. Natl. Cancer Inst. 96, 261–268.

Venesio, T., Balsamo, A., Errichiello, E., Ranzani, G.N., Risio, M., 2013. Oxidative DNA damage drives carcinogenesis in MUTYH-associated-polyposis by specific mutations of mitochondrial and MAPK genes. Mod. Pathol. 26, 1371–1381.

Weren, R.D., Ligtenberg, M.J., Kets, C.M., de Voer, R.M., Verwiel, E.T., Spruijt, L., van Zelst-Stams, W.A., Jongmans, M.C., Gilissen, C., Hehir-Kwa, J.Y., et al., 2015. Germline homozygous mutation in the base-excision repair gene NTHL1 causes adenomatous polyposis and colorectal cancer. Nat. Genet. 47, 668–671.